Sensors & Diagnostics

PAPER

View Article Online
View Journal | View Issue

Cite this: *Sens. Diagn.*, 2024, **3**, 448

A fluorescent sp^{2}c-covalent organic polymer with an aggregation-induced emission unit to suppress aggregation-induced quenching for sensing furazolidone†

Xinyi Wang, Lijuan Kuang, Meiling Ye, Liangmei Zou, Li Wang * and Yonghai Song *

Furazolidone (FZD) is a nitrofuran antibiotic that has an inhibitory effect on a variety of Gram-negative and positive bacteria. However, excessive use of FZD can produce major adverse responses and irreversible harm to the central nervous system, so it is necessary to develop a simple, rapid, highly selective and sensitive method for the detection of FZD. Here, a sp^{2}c-covalent organic polymer ($COP_{PDAN\text{-}BTT}$) containing benzotrithiophene was synthesized for fluorescence sensing FZD. The benzotrithiophene in the BTT monomer is a typical aggregation-induced quenching (ACQ) fluorophore, and the cyanide diphenylethylene unit has certain aggregation-induced emission (AIE) properties. The connection of the ACQ fluorophore and the AIE fluorophore can fully improve the ACQ degree of $COP_{PDAN\text{-}BTT}$. Under excitation at 370 nm, $COP_{PDAN\text{-}BTT}$ exhibits green fluorescence at 500 nm. Based on the internal filtering effect, $COP_{PDAN\text{-}BTT}$ was used for FZD detection. The I_0/I showed a good linear relationship with the concentration of FZD in the range of 0.034–20 μg mL^{-1} (0.149–88.9 μM), and the detection limit was as low as 0.011 μg mL^{-1} (0.049 μM). Based on the AIE properties of $COP_{PDAN\text{-}BTT}$, a fluorescent test strip was prepared for visual detection of FZD. This work provides a simple yet effective method for detection of FZD and improving the fluorescence of COPs.

Received 18th November 2023,
Accepted 24th January 2024

DOI: 10.1039/d3sd00307h

rsc.li/sensors

1. Introduction

Furazolidone (FZD) is a nitrofuran antibiotic that has an inhibitory effect on a variety of Gram-negative and positive bacteria and can be used to stimulate growth and treat a range of gastrointestinal diseases caused by bacterial and protozoal infections in poultry and aquaculture animals.[1] However, many studies have shown that FZD residues and their metabolites (3-amino-2-oxazolidinone) in foods cause potentially carcinogenic, mutagenic, and genotoxic effects. It can also damage the human liver and deoxyribonucleic acid (DNA) as well as inhibit cell growth.[2] Thus, it is necessary to develop a simple, rapid, highly selective and sensitive method for the detection of FZD residues.[3] At present, high performance liquid chromatography,[4] liquid chromatography-mass spectrometry,[5] triple tandem liquid chromatography-mass spectrometry[6] and enzyme-linked immunoassay[7] have been used for the detection of FZD. However, shortcomings such as time-consuming, expensive, and complex equipment, complicated sample preparation and difficulty in field inspection limit the wide application of the above traditional methods. Fluorescent sensors have attracted more and more attention because of their advantages such as simple operation, high sensitivity, good selectivity and strong visual recognition ability in recent years.[8–10]

Covalent organic polymers (COPs) are materials formed by stable covalent bonds with backbones composed of lightweight elements such as C, H, N, O, F, and S.[11–14] COPs have the advantages of structural diversity, large specific surface area, controllable chemical and physical properties, abundant π-conjugated systems, and various synthesis strategies.[15,16] In addition, they can interact well with other molecules through non-covalent interactions, so they can be widely used in gas separation and storage, energy storage, catalysis, energy conversion and sensing.[17,18] Compared with metal–organic frameworks (MOFs),[19] COPs connected by covalent bonds have higher stability. In addition, COPs are metal-free materials with excellent biocompatibility and low biotoxicity.[20] Therefore, COPs with extended π-conjugated main chains and high stability are widely used in the

College of Chemistry and Chemical Engineering, Jiangxi Normal University, 99 Ziyang Avenue, Nanchang 330022, China. E-mail: lwang@jxnu.edu.cn, yhsonggroup@hotmail.com, yhsong@jxnu.edu.cn

† Electronic supplementary information (ESI) available. See DOI: https://doi.org/10.1039/d3sd00307h

construction of fluorescent sensors.[21] However, the aggregate fluorescence quenching (ACQ) phenomenon is a serious obstruction in fluorescent sensors based on COPs.

Traditional luminescent groups with planarity and strong intermolecular interaction generally emit bright light in the monodisperse state, while the luminescence is weakened or even quenched in the aggregated state, which is called ACQ. Nevertheless, several strategies have been developed to improve the fluorescence of COPs. For example, Wang *et al.* designed and synthesized a hydrazine-linked TFBE-TD COP with yellow-green fluorescence. The COP exhibited a good backbone structure and aggregation-induced limitation of synergistic effects of tetraphenylene (TPE) molecules in the solid state, which resulted in improved fluorescence quantum yields of the relaxation.[22] Zhang *et al.* designed and synthesized a novel TPE-based COP by the Suzuki coupling reaction, which showed high selectivity. Meanwhile, some molecules emit weak or no light in dilute solution, but emit more light in the aggregated state or solid state. This phenomenon is called "aggregation-induced emission" (AIE). By connecting the AIE group with the traditional planar ACQ molecule,[23] the solid state luminescence of the molecule is promoted through the restricted intramolecular rotation process of the AIE unit,[24] the ACQ effect of the planar luminescent group is effectively eliminated, and the conversion from ACQ to AIE is realized.[25,26]

In this work, a sp^2c-covalent COP was synthesized by the Knoevenagel condensation reaction between benzo[1,2-*b*:3,4-*b*′:5,6-*b*″]trithiophene-2,5,8-tricarbaldehyde (BTT) and 1,4-phenylenediacetonitrile (PDAN). Cyanide diphenylethylene, which is the linkage unit in the sp^2c-covalent $COP_{PDAN\text{-}BTT}$, is an AIE active unit with a distorted conformation. The twisted molecular conformation originating from the steric hindrance between the neighboring phenyl rings and the nitrile moiety obstructs the intermolecular π–π stacking and thus prevents the emission quenching in the aggregated state.[27] Under excitation at 370 nm, the synthesized $COP_{PDAN\text{-}BTT}$ has greenish-yellow fluorescence emission at 500 nm. There was an inner filter effect (IFE) between $COP_{PDAN\text{-}BTT}$ and FZD, which significantly quenched the yellow-green fluorescence of $COP_{PDAN\text{-}BTT}$. Using $COP_{PDAN\text{-}BTT}$ as the fluorescent probe, the I_0/I showed a good linear relationship with the concentration of FZD in the range of 0.034–20 μg mL^{-1} (0.149–88.9 μM), with the lowest detection limit as low as 0.011 μg mL^{-1} (0.049 μM).[28]

2. Experimental section

2.1. Synthesis of $COP_{PDAN\text{-}BTT}$ and $COP_{PDAN\text{-}TF}$

For the preparation of $COP_{PDAN\text{-}BTT}$, BTT (0.1 mmol) and PDAN (0.15 mmol) were dissolved in a mixture of 2 mL mesitylene/1,4-dioxane (1 : 5), respectively. After complete dissolution by ultrasonication, the two solutions were transferred to a Schlenk tube with a capacity of 10 mL and mixed evenly. Then, NaOH (0.4 mL, 4 mol L^{-1}) solution was added as a catalyst. Next, the tube was frozen at 77 K (liquid N_2 bath) and degassed by three freeze–pump–thaw cycles. After that, the tube was sealed off and then heated at 120 °C for 3 days. After the reactor was cooled to room temperature, the precipitate was obtained by centrifugation at 10 000 rpm for 10 min. DMF and ethanol were added to wash the product to remove the unreacted reagent, and the above operation was repeated at least 3 times. After centrifugation, the yellow-brown product was obtained. The $COP_{PDAN\text{-}BTT}$ was dried in a freeze dryer for 6 h. In order to obtain good dispersion, the obtained $COP_{PDAN\text{-}BTT}$ was ground in an agate mortar.

As a comparison, $COP_{PDAN\text{-}TF}$ was also prepared. The preparation process of $COP_{PDAN\text{-}TF}$ is similar to that of $COP_{PDAN\text{-}BTT}$. Only BTT (0.1 mmol) was changed to TF (0.1 mmol), and the reaction solvent was changed to 1,4-dioxane, and finally a white powder was obtained. The synthesis process is shown in Scheme 1.

2.2. Fluorescence detection method

The $COP_{PDAN\text{-}BTT}$ and $COP_{PDAN\text{-}TF}$ powders (2.0 mg) were dissolved in PBS (1.0 mL) to prepare a solution (2.0 mg mL^{-1}). The concentration of FZD was determined by fluorescence titration in PBS with pH = 8 ($COP_{PDAN\text{-}BTT}$) and pH = 7 ($COP_{PDAN\text{-}TF}$) with COPs. The emission spectrum was recorded under 370 nm ($COP_{PDAN\text{-}BTT}$) and 350 nm ($COP_{PDAN\text{-}TF}$) excitation, and the emission peak intensities at 500 nm ($COP_{PDAN\text{-}BTT}$) and 430 nm ($COP_{PDAN\text{-}TF}$) were recorded and analyzed. Selectivity experiments were carried out using the above method. FZD was replaced with interferents, and the concentration of the interferents in the probe solution was 100 μg mL^{-1}, and the concentration of NF was 10 μg mL^{-1}.

2.3. Production of fluorescent test strips

Non-fluorescent filter paper was cut into 1 cm diameter discs and immersed in well-dispersed $COP_{PDAN\text{-}BTT}$ and $COP_{PDAN\text{-}TF}$ solutions at a concentration of 5 mg mL^{-1} for 6 h, then

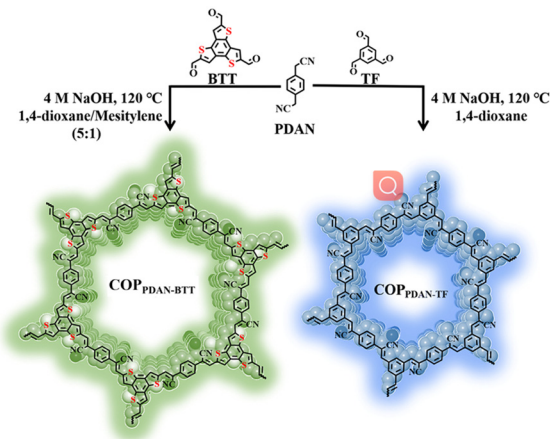

Scheme 1 Synthesis route of $COP_{PDAN\text{-}BTT}$ and $COP_{PDAN\text{-}TF}$.

removed and laid flat on Petri dishes and dried under an infrared lamp for subsequent experiments.

3. Results and discussion

3.1. Structural characterization of COPs

The morphology of COPs was characterized by scanning electron microscopy (SEM) and atomic force microscopy (AFM). It can be seen from the SEM images that both $COP_{PDAN\text{-}BTT}$ and $COP_{PDAN\text{-}TF}$ are ultra-thin two-dimensional lamellated structures (Fig. 1a and b). The thickness of $COP_{PDAN\text{-}BTT}$ and $COP_{PDAN\text{-}TF}$ measured by AFM was about 1.5 nm (Fig. 1d and e). The bonding, crystallinity and structure of $COP_{PDAN\text{-}BTT}$ and $COP_{PDAN\text{-}TF}$ were further characterized by FTIR, PXRD and N_2 adsorption/desorption isotherms. The FTIR spectrum of $COP_{PDAN\text{-}BTT}$ is shown in Fig. 1c. It was found that the C–H stretching vibration (2860 cm^{-1}) of the aldehyde group coming from BTT disappeared and the C=O stretching vibration (1670 cm^{-1}) of the aldehyde group decreased significantly. The –CH=C–CN formation caused an increase in π-electron delocalization, which shifted the C≡N stretching vibrational peak from 2249 cm^{-1} in PDAN to 2214 cm^{-1} in $COP_{PDAN\text{-}BTT}$. The change of the FTIR spectrum of $COP_{PDAN\text{-}TF}$ in Fig. S1a† is similar to that of $COP_{PDAN\text{-}BTT}$. There was a significant difference between the FTIR spectra of the COPs and their monomers, indicating the successful synthesis of the COPs.[29]

The crystallinity of $COP_{PDAN\text{-}BTT}$ and $COP_{PDAN\text{-}TF}$ was studied by powder X-ray diffraction (PXRD) (Fig. 1f).[30] $COP_{PDAN\text{-}BTT}$ has strong peaks at 6.68° and 7.30°, indicating that $COP_{PDAN\text{-}BTT}$ has good crystallinity. However, $COP_{PDAN\text{-}TF}$ has a wide diffraction peak at 20°, which indicates that $COP_{PDAN\text{-}TF}$ is amorphous. As shown in Fig. S2,† the N_2 adsorption/desorption isotherm of $COP_{PDAN\text{-}BTT}$ belongs to the typical type IV isotherm, while the N_2 adsorption/desorption isotherm of $COP_{PDAN\text{-}TF}$ belongs to the typical type II isotherm. The Brunauer–Emmett–Teller (BET) surface areas of $COP_{PDAN\text{-}BTT}$ and $COP_{PDAN\text{-}TF}$ are 117.9 $m^2\ g^{-1}$ and 110.2 $m^2\ g^{-1}$, respectively. According to the pore size distribution of $COP_{PDAN\text{-}BTT}$ and $COP_{PDAN\text{-}TF}$, the pore sizes of $COP_{PDAN\text{-}BTT}$ and $COP_{PDAN\text{-}TF}$ are 2.84 nm and 1.53 nm, respectively. The thermogravimetric analysis (TGA) of $COP_{PDAN\text{-}BTT}$ and $COP_{PDAN\text{-}TF}$ is shown in Fig. S3,† revealing their good thermal stability.

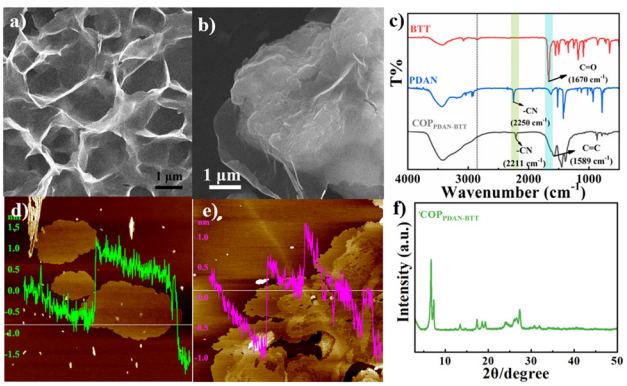

Fig. 1 SEM (a and b) and AEM (d and e) images of $COP_{PDAN\text{-}BTT}$ (a and d) and $COP_{PDAN\text{-}TF}$ (b and e). FTIR spectra of $COP_{PDAN\text{-}BTT}$ (c) and its monomers. XRD pattern of $COP_{PDAN\text{-}BTT}$ (f).

3.2. Optical properties of COPs

BTT with large conjugate planes tends to produce strong π–π interaction in the aggregated state, resulting in energy loss, and shows no or weak fluorescence, but green fluorescence can be observed in dilute solution (Fig. 2a). Due to their small conjugation degree, PDAN and TF, consisting of one benzene ring, exhibit weak fluorescence under 360 nm excitation (Fig. 2b and c).[31] Since the conjugation degree of $COP_{PDAN\text{-}TF}$ synthesized by TF and PDAN was significantly increased, strong blue fluorescence was observed at 430 nm and its CIE chromaticity coordinates were (0.1627, 0.1248) (Fig. 2e and f). It has been shown that the linking unit (cyanide diphenylethylene) is an AIE active unit with a non-planar twisted configuration. The π–π interactions between parallel cyanide diphenylethylene units in the two-dimensional COP plane can be confined by the large volume and strong polarity of –CN in cyanide diphenylethylene, resulting in *J*-aggregates with AIE activity. sp^2c-COPs with a cyanide stilbene structure as the connecting unit have certain AIE properties.[32] Under excitation at 400 nm (Fig. 2h), the $COP_{PDAN\text{-}TF}$ powder exhibits strong yellow-green fluorescence at 500 nm, and its CIE chromaticity coordinates are (0.3171, 0.3982) (Fig. 2i), which proves the existence of their AIE properties. In order to inhibit the ACQ properties of BTT,

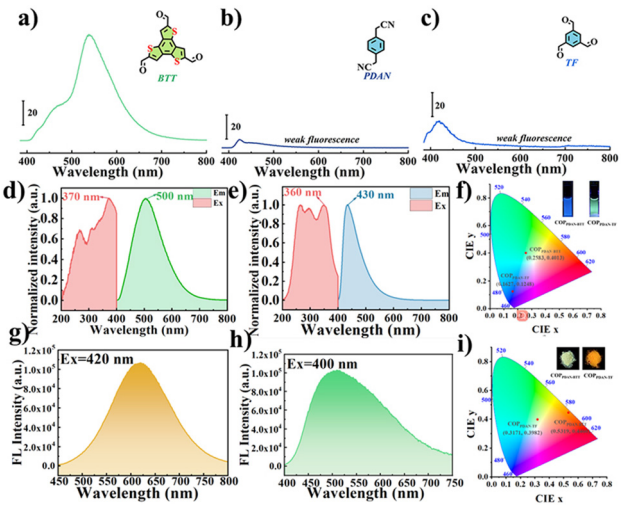

Fig. 2 Fluorescence spectra of aqueous solutions of (a) BTT, (b) PDAN and (c) TF. Fluorescence excitation and emission spectra of aqueous solutions of (d) $COP_{PDAN\text{-}BTT}$ and (e) $COP_{PDAN\text{-}TF}$. (f) CIE chromaticity diagrams of aqueous solutions of $COP_{PDAN\text{-}BTT}$ and $COP_{PDAN\text{-}TF}$. Fluorescence emission spectra of (g) $COP_{PDAN\text{-}BTT}$ and (h) $COP_{PDAN\text{-}TF}$ powders. (i) CIE chromaticity diagrams of $COP_{PDAN\text{-}BTT}$ and $COP_{PDAN\text{-}TF}$ powders. Insets: Photographs of $COP_{PDAN\text{-}BTT}$ and $COP_{PDAN\text{-}TF}$ under a UV lamp at 365 nm.

$COP_{PDAN-BTT}$ was synthesized with BTT and PDAN.[33] The aqueous solution of $COP_{PDAN-BTT}$ has green fluorescence at 500 nm (Fig. 2d), which is derived from the monomer BTT, with CIE chromaticity coordinates of (0.2583, 0.4013) (Fig. 2f). Under 420 nm excitation (Fig. 2g), the $COP_{PDAN-BTT}$ powder exhibited bright orange-yellow fluorescence with CIE chromaticity coordinates of (0.5319, 0.4460) (Fig. 2i). The strong solid fluorescence of $COP_{PDAN-BTT}$ indicates that $COP_{PDAN-BTT}$ has a significant AIE effect, that is, ACQ to AIE conversion is realized. Compared with the fluorescence in aqueous solution, the solid fluorescence of $COP_{PDAN-BTT}$ and $COP_{PDAN-TF}$ showed an obvious redshift phenomenon (Fig. 2).[34]

Then, the solubility of $COP_{PDAN-BTT}$ and $COP_{PDAN-TF}$ in different solvents was investigated. $COP_{PDAN-BTT}$ is well dispersed in water and partially dispersed in moderate-polar DMA and DMF, but it is completely insoluble in weakly polar THF (Fig. 3a). Under a 365 nm UV lamp, it can be observed that $COP_{PDAN-BTT}$ presents yellow-green fluorescence in aqueous solution, light yellow fluorescent and some orange fluorescent particles exist in DMA, scattered orange fluorescent particles exist in DMF, but orange fluorescent particles with obvious aggregation are found in THF (Fig. 3b).[35] The orange fluorescence of the orange fluorescent particles can be considered as solid fluorescence of $COP_{PDAN-BTT}$. The results show that $COP_{PDAN-BTT}$ has good solubility in strong polar solvent. As shown in Fig. 3d and e, compared with $COP_{PDAN-BTT}$, $COP_{PDAN-TF}$ was less decentralized. When $COP_{PDAN-TF}$ was dispersed in water, it showed blue fluorescence.[36] With the decrease of polarity, the solubility decreased gradually. As shown in Fig. S4,† the stability of $COP_{PDAN-TF}$ is poor due to its easy re-aggregation in solution, and the Tyndall effect is weak. The standard deviation of the fluorescence emission peaks at 430 nm was 36.2038. However, $COP_{PDAN-BTT}$ had good dispersion and an obvious Tyndall effect. The standard deviation of the fluorescence emission peaks at 500 nm was 0.7071. The good solubility of $COP_{PDAN-BTT}$ in water can be attributed to the presence of a large number of cyanide groups in the COP skeleton. As COPs are composed of a large number of benzene rings, generally speaking, the solubility of COPs in water is very poor, while the good solubility of sp^2c-COPs in water provides convenient conditions for the detection of FZD in the actual environment.[37]

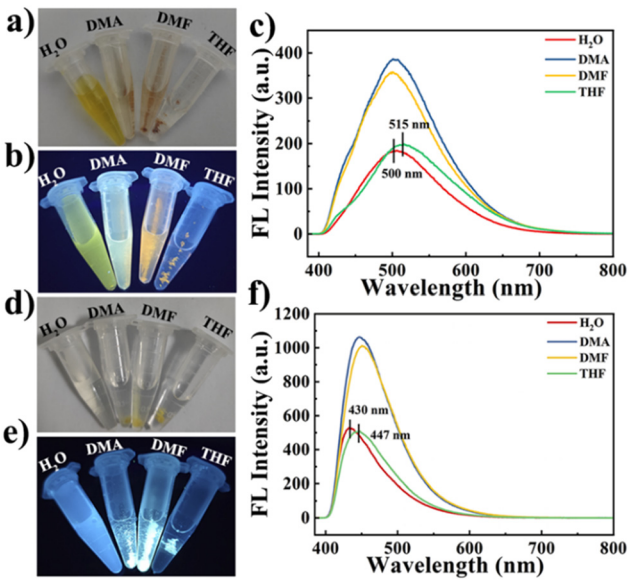

Fig. 3 Photographs of $COP_{PDAN-BTT}$ dissolved in different solvents (from left to right: H_2O, DMA, DMF and THF) under visible light (a) and a UV lamp (b). (c) Fluorescence emission spectra of $COP_{PDAN-BTT}$ in different solvents. $COP_{PDAN-TF}$ dissolved in different solvents (from left to right: H_2O, DMA, DMF and THF) under visible light (d) and a UV lamp (e). (f) Fluorescence emission spectra of $COP_{PDAN-TF}$ in different solvents. The dissolution concentration is 1 mg mL^{-1} (a, b, d and e) and the fluorescence test concentration is 120 μg mL^{-1} (c and f).

Then the fluorescence properties of $COP_{PDAN-BTT}$ and $COP_{PDAN-TTF}$ in different solvents were studied. As shown in Fig. 3c, the fluorescence intensity of $COP_{PDAN-BTT}$ in water was significantly lower than that in DMA and DMF. This is attributed to the AIE properties of $COP_{PDAN-BTT}$, that is, in a medium-polar solvent due to low solubility, $COP_{PDAN-BTT}$ agglomerates into small particles suspended in a solution and accordingly the fluorescence is enhanced greatly. In addition, in water the fluorescence emission peak of $COP_{PDAN-BTT}$ was at 500 nm, but in THF the fluorescence emission peak of $COP_{PDAN-BTT}$ was at 515 nm. The blueshift with increasing polarity can be attributed to the intramolecular charge transfer (ICT) nature of $COP_{PDAN-BTT}$, where the cyanide group of $COP_{PDAN-BTT}$ is a strong electron-absorbing group and benzotrithiophene is an electron-donating group, and there is an ICT effect from benzotrithiophene to cyano. The binding of the electron donor to the solvent weakens the ability to drive electrons and reduces the charge separation of the system, resulting in a blue shift. The case of $COP_{PDAN-TTF}$ is similar to that of $COP_{PDAN-BTT}$. The cyanide group of $COP_{PDAN-TF}$ is a strong electron-absorbing group, and the benzene ring is an electron-giving group, and there exists an ICT effect. In THF, the fluorescence emission peak of $COP_{PDAN-TF}$ is positioned at 447 nm, while with increasing polarity, the fluorescence emission peak of $COP_{PDAN-TF}$ in water is blue-shifted to 430 nm (Fig. 3f).[38]

To verify the AIE properties of $COP_{PDAN-BTT}$ and $COP_{PDAN-TF}$, the fluorescence emission of $COP_{PDAN-BTT}$ and $COP_{PDAN-TF}$ in solvents with different viscosities was further examined. The conversion of AIE molecules from weak fluorescence in the single-molecule state to strong fluorescence in the aggregated state is achieved through restricted intramolecular motion. Therefore, in high-viscosity solvents, AIE molecules exhibit enhanced fluorescence due to restricted vibration or rotation. Glycerol alcohol is a liquid with high viscosity (800 at 25 °C). Solutions with different viscosities can be obtained by mixing glycerol and water in different proportions. As shown in Fig. S5,† with the enhancement of viscosity, the fluorescence of $COP_{PDAN-BTT}$

and $COP_{PDAN\text{-}TF}$ is gradually limited in intramolecular vibration and rotation, and the fluorescence shows an increasing trend. Therefore, the results show that $COP_{PDAN\text{-}BTT}$ and $COP_{PDAN\text{-}TF}$ have AIE properties.

3.3. Sensing performance of $COP_{PDAN\text{-}BTT}$ and $COP_{PDAN\text{-}TF}$ for FZD

In order to obtain better detection results, the amount of probe and the pH of the detection environment were optimized (Fig. S6†). The fluorescence responses of $COP_{PDAN\text{-}BTT}$ and $COP_{PDAN\text{-}TF}$ to FZD were studied under the above optimized conditions.[39] As shown in Fig. 4a, with the increase of the concentration of FZD, the fluorescence of $COP_{PDAN\text{-}BTT}$ at 500 nm was continuously quenched, and the fluorescence emission peak of $COP_{PDAN\text{-}TF}$ at 430 nm was continuously decreased (Fig. 4d). As shown in Fig. 4b, FZD was detected in the concentration range of 0.034–20 μg mL^{-1} (0.149–88.9 μM) with a good linear relationship between I_0/I and the concentration of FZD, and the detection limit was as low as 0.011 μg mL^{-1} (0.049 μM) at S/R = 3. As shown in Fig. 4e, two linear relationships were obtained for FZD in the concentration range of 0.069–14 μg mL^{-1} (0.307–62.2 μM) and 14–28 μg mL^{-1} (62.2–124.4 μM), respectively. The I_0/I of $COP_{PDAN\text{-}TF}$ obtained two linear relationships with the corresponding detection limit of 0.023 μg mL^{-1} (0.101 μM), which was lower than that of $COP_{PDAN\text{-}BTT}$. Compared with other analytical methods and other reported FZD fluorescent sensors, $COP_{PDAN\text{-}BTT}$ and $COP_{PDAN\text{-}TF}$ both have better detection performance (Table S1†). To evaluate the selectivity of $COP_{PDAN\text{-}BTT}$ and $COP_{PDAN\text{-}TF}$ for FZD detection, we added FZD and some potential interfering substances (Na^+, K^+, Ag^+, Fe^{3+}, Al^{3+}, Hg^{2+}, EF, AA, L-dopa, *t*BHQ, AMX, AK, MT, FT) to a series of blank fluorescent probe solutions, respectively, and the corresponding fluorescence intensity changes were recorded. Apparently, there was no significant quenching of the fluorescence of $COP_{PDAN\text{-}BTT}$ and $COP_{PDAN\text{-}TF}$ in the presence of other interfering substances, indicating that $COP_{PDAN\text{-}BTT}$ and $COP_{PDAN\text{-}TF}$ have high selectivity for FZD fluorescence detection (Fig. 4c and f).[40]

The fluorescent colorimetric test strip can be used to observe the fluorescence brightness and color change by the naked eye, which has a better field survey effect. Using the AIE properties of $COP_{PDAN\text{-}BTT}$ and $COP_{PDAN\text{-}TF}$, $COP_{PDAN\text{-}BTT}$ and $COP_{PDAN\text{-}TF}$ were fixed on filter paper to make portable test strips for visualization of FZD. Fig. 5 shows a test strip under UV lamp irradiation at 365 nm and bright green and blue fluorescence appeared. 5 μL of different concentrations of FZD solution (0.2, 0.4, 0.6, 0.8, 1.0, 1.2, 1.5 mg mL^{-1}) were dropped on the test strips, and both $COP_{PDAN\text{-}BTT}$ and $COP_{PDAN\text{-}TF}$ test strips showed a significant change from bright to dark with the increase of FZD concentration. At the same FZD concentration, compared with $COP_{PDAN\text{-}TF}$, the quenching of $COP_{PDAN\text{-}BTT}$ was more significant.[41]

3.4. Detection mechanism of $COP_{PDAN\text{-}BTT}$ and $COP_{PDAN\text{-}TF}$ for FZD

The mechanism of FZD quenching luminescence was further investigated by fluorescence spectra and UV-vis absorption spectra. According to previous work, there are two possible mechanisms for the detection of FZD by $COP_{PDAN\text{-}BTT}$ and $COP_{PDAN\text{-}TF}$: fluorescence resonance energy transfer (FRET) and internal filtering effect (IFE).[42] An obvious absorption peak of FZD can be observed at 375 nm, and the fluorescence emission peaks of $COP_{PDAN\text{-}BTT}$ and $COP_{PDAN\text{-}TF}$ are at 500 nm and 430 nm, respectively, without obvious overlap with the UV absorption peaks of FZD (Fig. 6a and c).[43] The possible mechanism of fluorescence resonance energy transfer (FRET) is ruled out. However, the excitation wavelengths of $COP_{PDAN\text{-}BTT}$ and $COP_{PDAN\text{-}TF}$ were 370 nm and 350 nm,

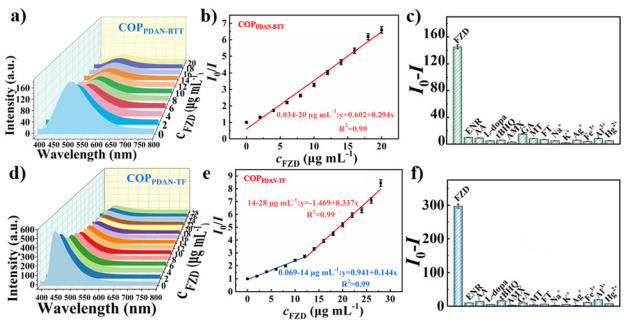

Fig. 4 (a) Fluorescence emission spectra after the addition of different concentrations of FZD to $COP_{PDAN\text{-}BTT}$ (λ_{ex} = 370 nm). (b) Linear plot between the FZD concentration and I_0/I. (c) Fluorescence emission spectra of $COP_{PDAN\text{-}BTT}$ in the presence of FZD and other interferents (Na^+, K^+, Ag^+, Fe^{3+}, Al^{3+}, Hg^{2+}, ENR, AA, L-dopa, tBHQ, AMX, AK, MT, FT). (d) Fluorescence emission spectra (λ_{ex} = 350 nm) after the addition of different concentrations of FZD to $COP_{PDAN\text{-}TF}$. (e) Linear plot between the FZD concentration and I_0/I. (f) Fluorescence emission spectra of $COP_{PDAN\text{-}TF}$ in the presence of FZD and other interferents (Na^+, K^+, Ag^+, Fe^{3+}, Al^{3+}, Hg^{2+}, ENR, AA, L-dopa, *t*BHQ, AMX, AK, MT, FT). The concentration of FZD was 10 μg mL^{-1} and the concentration of all other interferents was 100 μg mL^{-1}.

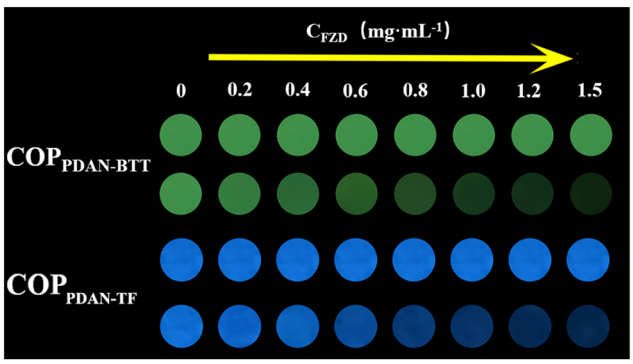

Fig. 5 After 5 μL of different concentrations of FZD solution (0.2, 0.4, 0.6, 0.8, 1.0, 1.2, 1.5 mg mL^{-1}) were dropped on the test strips, fluorescence changes of $COP_{PDAN\text{-}BTT}$ and $COP_{PDAN\text{-}TF}$ test paper with the addition of FZD under a UV lamp at 365 nm.

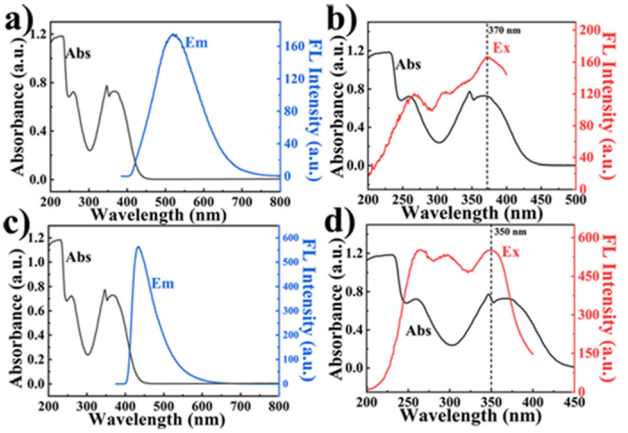

Fig. 6 (a) Fluorescence emission spectrogram of $COP_{PDAN\text{-}BTT}$ and UV-vis absorption spectra of FZD. (b) Fluorescence excitation spectrogram of $COP_{PDAN\text{-}BTT}$ and UV-vis absorption spectra of FZD. (c) Fluorescence emission spectrogram of $COP_{PDAN\text{-}TF}$ and UV-vis absorption spectra of FZD. (d) Fluorescence excitation spectrogram of $COP_{PDAN\text{-}TF}$ and UV-vis absorption spectra of FZD.

respectively, which were in the range of the UV absorption peak of FZD. This proved that the quenching mechanism of $COP_{PDAN\text{-}BTT}$ and $COP_{PDAN\text{-}TF}$ on FZD was the IFE (Fig. 6b and d).[44]

3.5. Detection of FZD in the actual samples

We examined the FZD residues in lake water samples using $COP_{PDAN\text{-}BTT}$ and $COP_{PDAN\text{-}TF}$, respectively. The samples were filtered with filter paper to remove the solid impurities in the lake water before testing, and then different concentrations of FZD (5, 10, 20 μg mL^{-1}) were added to the samples using the standard addition method for the determination. The results showed that there was no significant FZD residue in the lake water, and the spiked recoveries were within 95.8–102.6% (Table S2†).

4. Conclusions

In summary, we have successfully synthesized $COP_{PDAN\text{-}BTT}$ by the Knoevenagel reaction. BTT and PDAN were selected to synthesize $COP_{PDAN\text{-}BTT}$ with AIE properties for the first time, which achieves the conversion from ACQ to AIE and is used to detect FZD. Under 370 nm excitation, the yellow-green fluorescence emission of $COP_{PDAN\text{-}BTT}$ was present at 500 nm. The addition of FZD quenched the yellow-green fluorescence of $COP_{PDAN\text{-}BTT}$ due to the presence of the IFE with FZD. Using $COP_{PDAN\text{-}BTT}$ as the fluorescent probe, the I_0/I showed a good linear relationship with the concentration of FZD in the range of 0.034–20 μg mL^{-1} (0.149–88.9 μM), with the lowest detection limit as low as 0.011 μg mL^{-1} (0.049 μM). Thus, $COP_{PDAN\text{-}BTT}$ showed great activity with a lower detection limit, wide linear range, good interference and stability for FZD detection. The AIE properties were used to produce test strips for the visualization of FZD. With these excellent properties, the proposed test strips could be applied for future analytical applications in real-world samples, such as residual furazolidones in aquaculture.

Author contributions

Xinyi Wang: data analysis, resources, investigation, writing – original draft. Lijuan Kuang: methodology, validation. Meiling Ye: investigation. Liangmei Zou: investigation. Li Wang: methodology, writing – review & editing, supervision. Yonghai Song: conceptualization, funding acquisition, supervision, writing – review & editing.

Conflicts of interest

The authors declare that they have no conflicts of interest.

Acknowledgements

This work was financially supported by the National Natural Science Foundation of China (21665012, 21765009, 21964010, and 22264016).

References

1 N. Riswana Barveen, T.-J. Wang and Y.-H. Chang, *Chem. Eng. J.*, 2021, **423**, 130191.
2 E. A. Kumar, T. Kokulnathan, T.-J. Wang, K. M. A. Kumar and Y.-H. Chang, *J. Environ. Chem. Eng.*, 2023, **11**, 1706–1712.
3 S. Zhang, Y. Mao, T. Song, X. Zhao, Z. Song and W. Wang, *Carbon*, 2023, **213**, 118213.
4 R. S. van den Hurk, M. Pursch, D. R. Stoll and B. W. J. Pirok, *TrAC, Trends Anal. Chem.*, 2023, **166**, 117166.
5 M. F. Zaki, Y.-H. Wu, P.-C. Chen and P.-S. Chen, *Sens. Actuators, B*, 2023, **393**, 134243.
6 R. S. Minhas, D. A. Rudd, H. Z. Al Hmoud, T. M. Guinan, K. P. Kirkbride and N. H. Voelcker, *ACS Appl. Mater. Interfaces*, 2020, **12**, 31195–31204.
7 N. Li, H. Chen, M. Zhang, Y. Zha, Z. Mu, Y. Ma and P. Chen, *Sens. Actuators, B*, 2020, **315**, 128135.
8 M. Li, H. Wan, J. Xiong, L. Wang, L. Yang, L. Wang and Y. Song, *Chem. Eng. J.*, 2023, **468**, 143538.
9 S. Wang, L. Guo, L. Chen, L. Wang and Y. Song, *ACS Appl. Nano Mater.*, 2022, **5**, 1339–1347.
10 L. Yang, M. Li, L. Kuang, Y. Li, L. Chen, C. Lin, L. Wang and Y. Song, *Biosens. Bioelectron.*, 2022, **214**, 114527.
11 L. Guo and D. Cao, *J. Mater. Chem. C*, 2015, **3**, 8490–8494.
12 H. Zhang, J. Zhou, G.-G. Shan, G.-F. Li, C.-Y. Sun, D.-X. Cui, X.-L. Wang and Z.-M. Su, *Chem. Commun.*, 2019, **55**, 12328–12331.
13 E. Özdemir, D. Thirion and C. T. Yavuz, *RSC Adv.*, 2015, **5**, 69010–69015.
14 G. Das, T. Prakasam, S. Nuryyeva, D. S. Han, A. Abdel-Wahab, J.-C. Olsen, K. Polychronopoulou, C. Platas-Iglesias, F. Ravaux, M. Jouiad and A. Trabolsi, *J. Mater. Chem. A*, 2016, **4**, 15361–15369.

15 K. Prakash Subodh and D. T. Masram, *J. Mater. Chem. C*, 2020, **8**, 9201–9204.
16 D. Yadav and S. K. Awasthi, *Green Chem.*, 2020, **22**, 4295–4303.
17 Y. Chen, W. Li, R.-Z. Gao, X.-H. Wang, A.-N. Tang and D.-M. Kong, *J. Mater. Chem. C*, 2022, **10**, 1236–1245.
18 S. Qu, N. Song, G. Xu and Q. Jia, *Sens. Actuators, B*, 2019, **290**, 9–14.
19 Y.-Q. Sun, Y. Cheng and X.-B. Yin, *Anal. Chem.*, 2021, **93**, 3559–3566.
20 L. Guo, L. Yang, M. Li, L. Kuang, Y. Song and L. Wang, *Coord. Chem. Rev.*, 2021, **440**, 213957.
21 L. Yang, Y. Song, C. Lin, L. Hou, L. Guo, Y. Lei and L. Wang, *Sens. Actuators, B*, 2021, **341**, 129995.
22 R. Wang, C. He, Z. Xu, Y. Lei, Y. Jiang, J. Zhang, S. Chen and D. Zhang, *Dyes Pigm.*, 2022, **206**, 24570–24579.
23 D. Hu, H. Huang, R. Li, J. Yuan and Y. Wei, *Sci. China: Chem.*, 2022, **65**, 1532–1537.
24 Z. Gong, X. Rong, G. Sui, X. Jiang, M. Xu, C. Wang and S. Meng, *Adv. Opt. Mater.*, 2023, **11**, 2203075.
25 S. Dalapati, E. Jin, M. Addicoat, T. Heine and D. Jiang, *J. Am. Chem. Soc.*, 2016, **138**, 5797–5800.
26 P. Albacete, J. I. Martínez, X. Li, A. López-Moreno, S. a. Mena-Hernando, A. E. Platero-Prats, C. Montoro, K. P. Loh, E. M. Pérez and F. Zamora, *J. Am. Chem. Soc.*, 2018, **140**, 12922–12929.
27 J. Mei, N. L. C. Leung, R. T. K. Kwok, J. W. Y. Lam and B. Z. Tang, *Chem. Rev.*, 2015, **115**, 11718–11940.
28 Z. Cong, Z. Song, Y. Ma, M. Zhu, Y. Zhang, S. Wu and E. Gao, *Chem. – Asian J.*, 2021, **16**, 1773–1779.
29 R. Chen, J. L. Shi, Y. Ma, G. Lin, X. Lang and C. Wang, *Angew. Chem., Int. Ed.*, 2019, **58**, 6430–6434.
30 S. Ballur Prasanna, R. Sakthivel, L.-Y. Lin, Y.-F. Duann, J.-H. He, T.-Y. Liu and R.-J. Chung, *Appl. Surf. Sci.*, 2023, **611**, 155784.
31 C. Huang, S. Zhou, C. Chen, X. Wang, R. Ding, Y. Xu, Z. Cheng, Z. Ye, L. Sun, Z. J. Wang, D. Hu, X. Jia, G. Zhang and S. Gao, *Small*, 2022, **18**, 220506.
32 G.-J. Li, J.-L. Ni, A. Mensah, M. Li, L.-Z. Chen and F.-M. Wang, *J. Porous Mater.*, 2022, **29**, 1531–1538.
33 Y. Cai, H. Zhu, W. Zhou, Z. Qiu, C. Chen, A. Qileng, K. Li and Y. Liu, *Anal. Chem.*, 2021, **93**, 7275–7282.
34 Y. Shen, Y. Wei, C. Zhu, J. Cao and D.-M. Han, *Coord. Chem. Rev.*, 2022, **458**, 759–770.
35 H. Sun, X. Li, Z. Hu, C. Gu, D. Chen, J. Wang, B. Li, T. Jiang and X. Zhou, *Appl. Surf. Sci.*, 2021, **556**, 149748.
36 H. Tan and Y. Li, *Microchim. Acta*, 2021, **188**, 254–263.
37 J. Yang, Y. Cao, W. Si, J. Zhang, J. Wang, Y. Qu and W. Qin, *ChemSusChem*, 2022, **15**, 578496.
38 Y. Yang, J. Chen, Z. Chen, Z. Yu, J. Xue, T. Luan, S. Chen and S. Zhou, *Water Res.*, 2022, **223**, 118979.
39 X. Yue, Z. Zhou, M. Li, M. Jie, B. Xu and Y. Bai, *Food Chem.*, 2022, **367**, 130763.
40 J. Zhang, F. Xue and Z. Wang, *Chem. Mater.*, 2022, **34**, 10701–10710.
41 Z. Zhao, H. Zhang, J. W. Y. Lam and B. Z. Tang, *Angew. Chem., Int. Ed.*, 2020, **59**, 9888–9907.
42 Z. Gao, M. Liu, K. Xu, M. Tang, X. Lin, S. Hu and X. Ren, *Anal. Methods*, 2020, **12**, 2551–2554.
43 Q.-X. Luo, W.-R. Cui, Y.-J. Li, Y.-J. Cai, X.-L. Mao, R.-P. Liang and J.-D. Qiu, *ACS Appl. Electron. Mater.*, 2021, **3**, 4490–4497.
44 X. Niu, X. Bo and L. Guo, *Food Chem.*, 2021, **364**, 130368.